AGU PUBLICATIONS

Paleoceanography

RESEARCH ARTICLE
10.1002/2014PA002633

Key Points:
- Downcore records of Pa/Th and sortable silt are compared for three cores
- All three cores record Pa/Th above the production ratio during Heinrich Stadial 1
- Both advection slowdown and boundary scavenging are inferred

Supporting Information:
- Readme
- Figure S1
- Figure S2
- Text S1
- Table S1
- Table S2

Correspondence to:
N. L. Roberts,
nr297@cam.ac.uk

Citation:
Roberts, N. L., J. F. McManus, A. M. Piotrowski, and I. N. McCave (2014), Advection and scavenging controls of Pa/Th in the northern NE Atlantic, *Paleoceanography*, *29*, 668–679, doi:10.1002/2014PA002633.

Received 21 FEB 2014
Accepted 23 MAY 2014
Accepted article online 2 JUN 2014
Published online 30 JUN 2014

Advection and scavenging controls of Pa/Th in the northern NE Atlantic

Natalie L. Roberts[1], Jerry F. McManus[2], Alexander M. Piotrowski[1], and I. Nicholas McCave[1]

[1]Godwin Laboratory for Paleoclimate Research, Department of Earth Sciences, Cambridge, UK, [2]Department of Earth and Environmental Science, Lamont-Doherty Earth Observatory of Columbia University, Palisades, New York, USA

Abstract Over the last 2 decades, significant advances have been made in reconstructing past rates of ocean circulation using sedimentary proxies for the dynamics of abyssal waters. In this study we combine the use of two rate proxies, sortable silt grain size, and sedimentary $^{231}Pa/^{230}Th$, measured on a depth transect of deep-sea sediment cores from the northern NE Atlantic, to investigate ocean circulation changes during the last deglacial. We find that at two deep sites, the core-top $^{231}Pa/^{230}Th$ ratios reflect Holocene circulation rates, while during Heinrich Stadial 1, the deglacial ratios peaked as the sortable silt grain size decreased, reflecting a general circulation slowdown. However, the peak $^{231}Pa/^{230}Th$ significantly exceeded the production ratio in both cores, indicating that $^{231}Pa/^{230}Th$ was only partially controlled by ocean circulation at these sites. This is supported by a record of $^{231}Pa/^{230}Th$ from an intermediate water depth site, where values also peaked during Heinrich Stadial 1, but were consistently above the production ratio over the last 24 ka, reflecting high scavenging below productive surface waters. At our study sites, we find that preserved sediment component fluxes cannot be used to distinguish between a scavenging or circulation control, although they are consistent with a circulation influence, since the core at intermediate depth with the highest $^{231}Pa/^{230}Th$ recorded the lowest particle fluxes. Reconstruction of advection rate using $^{231}Pa/^{230}Th$ in this region is complicated by high productivity, but the data nevertheless contain important information on past deep ocean circulation.

1. Introduction

Proxy records from the North Atlantic indicate that abrupt climate changes, such as Heinrich events and Dansgaard-Oeschger cycles, are associated with freshwater input and upper ocean stratification [e.g., *Benway et al.*, 2010; *Dokken and Jansen*, 1999; *Hemming et al.*, 1998; *Thornalley et al.*, 2011; *Waelbroeck et al.*, 2001]. Modeling experiments have demonstrated that localized freshwater input to the northern high latitudes would perturb deep water formation and result in a weaker meridional ocean circulation [e.g., *Ganopolski and Ramstorf*, 2001; *LeGrande et al.*, 2006; *Liu et al.*, 2009; *Peltier et al.*, 2006], leading to reduced northward oceanic heat transport and cooling of the northern hemisphere [*Clark et al.*, 2002; *Manabe and Stouffer*, 1997; *Timmermann et al.*, 2005; *Vellinga and Wood*, 2002; *Zhang and Delworth*, 2005]. Understanding the degree to which ocean circulation weakened during these events is essential for predicting future ocean-climate responses to freshwater forcing and for estimating past carbon storage and ventilation of the deep ocean [*Kwon et al.*, 2012]. This study is the first to compare two rate proxies measured on the same suite of cores: (i) sedimentary $(^{231}Pa_{ex}/^{230}Th_{ex})_0$ (excess ^{231}Pa and ^{230}Th activity ratio decay corrected to the time of deposition, $^{231}Pa/^{230}Th$ hereafter), which was first proposed as a proxy for the rate of ocean circulation by *Yu et al.* [1996], and (ii) sortable silt mean grain size ($\overline{SS}$ hereafter), pioneered by *McCave et al.* [1995b].

Radionuclides ^{231}Pa and ^{230}Th are produced uniformly in seawater by decay of ^{235}U and ^{238}U, respectively, at a constant initial $^{231}Pa/^{230}Th$ activity ratio of 0.093. Both ^{231}Pa and ^{230}Th have short residence times of ~100–200 years and 10–40 years [*Henderson and Anderson,* 2003; *Yu et al.,* 1996], respectively, relative to whole ocean overturn due to their high reactivity and removal by chemical scavenging onto sinking particles [*Anderson et al.*, 1983a]. The use of sedimentary $^{231}Pa/^{230}Th$ as an advection proxy relies on two factors: (i) ^{230}Th is dominantly vertically scavenged at the site of production [*Anderson et al.*, 1983a], while (ii) ^{231}Pa is largely advected away from the site of production [*Yu et al.*, 1996] and is then removed by adsorption in regions of high scavenging intensity due to elevated particle flux and/or opal rain [*Anderson et al.*, 1983b; *Chase et al.*, 2002; *Henderson and Anderson*, 2003], often at ocean margins and in the Southern Ocean. The rate at which ^{231}Pa is transported by water masses relative to ^{230}Th has been suggested to play an

important role in determining the sedimentary $^{231}Pa/^{230}Th$ of Atlantic cores on a basin-wide scale [*Marchal et al.*, 2000; *McManus et al.*, 2004; *Yu et al.*, 1996]. However, recent studies suggest that local influences such as sediment flux [*Lippold et al.*, 2012b], particle composition [*Bradtmiller et al.*, 2006; *Kretschmer et al.*, 2011; *Scholten et al.*, 2008], and grain size [*Kretschmer et al.*, 2010; *McGee et al.*, 2010] may also influence Atlantic sedimentary $^{231}Pa/^{230}Th$ records. The relative importance of these influences needs to be assessed at each site before the $^{231}Pa/^{230}Th$ records can be interpreted in terms of ocean circulation rates.

The mean grain size of the sortable silt fraction ($\overline{SS}$) in sediments has been used as a proxy for bottom flow speed and hence the rate of ocean circulation based on the principle that high-current velocities are more able to suppress deposition of finer grains than low velocity currents, leading to a coarse mean grain size [*McCave et al.*, 1995a, 1995b]. The mean size of the redeposited silt (within the 10–63 μm fraction that mainly behaves as single particles [*Mehta and Letter*, 2013]) is found to be proportional to the local current velocity [*Ledbetter*, 1986; *McCave and Hall*, 2006]. As long as the sediment has been subject to many episodes of resuspension and deposition, the fine fraction properties reflect dynamical current control rather than the mode of introduction, such as ice rafting or wind. Ice rafting is recognized through the nonmobile coarse fraction, while wind-blown dust may be diagnosed through end-member modeling of the grain size spectra [*McCave et al.*, 1995a; *Stuut et al.*, 2002]. Because their respective influences are clearly different, the comparison of sortable silt and $^{231}Pa/^{230}Th$ records has great potential to provide complementary and robust information on the dynamics of deep ocean circulation.

Previous studies have also pointed out the importance of circulation changes at different depths in the water column [*Bertram et al.*, 1995; *Duplessy et al.*, 1988; *Gherardi et al.*, 2005, 2009; *Hall et al.*, 2006; *Lippold et al.*, 2012a; *McCave et al.*, 1995b; *Oppo and Lehman*, 1993]. In this study we compare $^{231}Pa/^{230}Th$ with ^{230}Th-normalized fluxes [*Francois et al.,* 2004] and previously published $\overline{SS}$ records [*McCave et al.*, 1995a] taken from an approximate depth transect of cores, sampling the principal water masses within a region of relatively high-particle flux, in order to distinguish between advection and scavenging controls on sedimentary $^{231}Pa/^{230}Th$. We then discuss the possible sources of dissolved ^{231}Pa to the northern NE Atlantic and the implications of boundary scavenging versus circulation as influences on its burial during the last deglacial.

2. Materials and Methods

2.1. Location

The sediment cores analyzed in this study were recovered from UK Biogeochemical Ocean Flux Study (BOFS) sites between 52–58°N and 16–22°W and 1150–4045 m water depth in the northeast Atlantic Ocean [*McCave*, 1989, Figure 1]. They are positioned atop and along the southern flank of the Rockall Plateau, just south of the Iceland-Faroe Ridge and the Faroe-Shetland Channel, allowing the potential for reconstructing changes in the rate of overflow waters exported from the Nordic Seas and their contribution to northern source deep and intermediate waters. As an approximate depth transect, this suite of cores permits us to sample different water masses and to monitor the integration of $^{231}Pa/^{230}Th$ through the water column by reversible scavenging [*Bacon and Anderson*, 1982; *McManus et al.*, 2004] on cores which have scavenging controls that are as similar as possible. Today, all three core sites are bathed by a similar mixture of different northern source component waters from the Nordic Seas and Labrador basin (Figure 1). During the Last Glacial Maximum (LGM), however, the North Atlantic water column was highly stratified [*Curry and Oppo,* 2005; *Duplessy et al.*, 1988; *Lynch-Stieglitz et al.*, 2007; *Oppo and Lehman*, 1993; *Sarnthein et al.*, 1995], and the three study sites were bathed by separate water masses previously determined using benthic $\delta^{13}C$ and B/Ca ratios measured on *Cibicidoides wuellerstorfi*, the deepest site bathed primarily by southern sourced water and the two shallower sites bathed by northern sourced water originating from two different dense water formation processes and possibly locations [*Yu et al.,* 2008].

2.2. Age Models

Manighetti et al. [1995] first developed age models for cores BOFS 17 K, 10 K, and 8 K by correlating planktonic oxygen isotopes, *X*-radiographs, and bulk magnetic susceptibilty peaks with core BOFS 5 K, which had been radiocarbon dated. The age models for BOFS 5 K, 8 K, and 17 K were later revised by *Barker et al.* [2004] using benthic $\delta^{18}O$ [*Bertram et al.*, 1995], percent sinistral *N. pachyderma*, and percent ice-rafted detritus (IRD) counts. Here we have adjusted the age models for each core based on new and previously

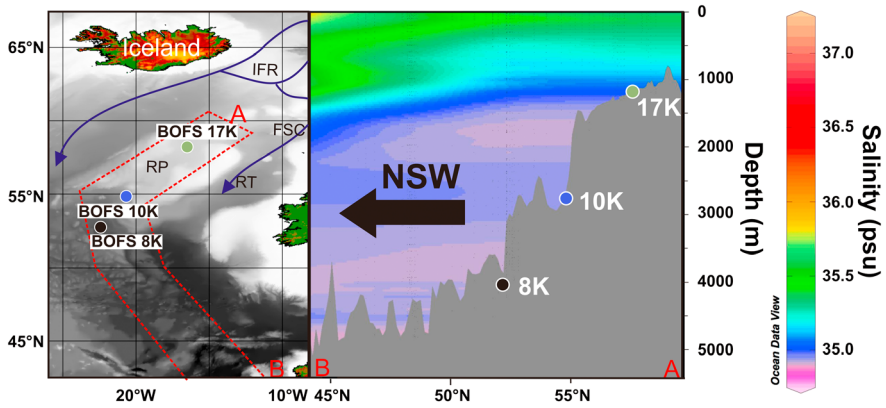

Figure 1. (left) A map of the northern NE Atlantic illustrating a schematic flow path of overflow waters (blue arrows) across the Iceland-Faroe Ridge, through the Faroe-Scotland Channel and into the area of the Rockall Trough and Rockall Plateau. Overflow waters along with Labrador Sea water then make up the northern source water (black arrow) which flows southward. The locations of the BOFS cores are displayed on the map and on the vertical cross section highlighted by the dashed red lines: 17 K (green: 58°0′N, 16°5′W, 1150 m), 10 K (blue: 54°7′N, 20°7′W, 2777 m), and 8 K (black: 52°5′N, 22°1′W, 4045 m).

published radiocarbon data [*Brown et al.,* 2001] not incorporated into previous age models (Table S1 in the supporting information).

All samples picked for radiocarbon dating were graphitized at the University of Cambridge, and the samples were run at the Australian National University Research School of Earth Sciences geochronology unit, using a National Electrostatic Corporation single-stage accelerator mass spectrometer. The radiocarbon dates were corrected for surface reservoir age effects based on calculations for preanthropogenic modern foraminifera ages [*Bard*, 1988] and on LGM samples from a nearby core [DAPC2, 58°58.10′N, 09°36.75′W, 1709 m; *Knutz et al.*, 2007]. The radiocarbon dates were then calibrated to calendar ages before present using the OXcal program (version 4.1 [*Ramsey*, 2001] and the Intcal04 calibration curve [*Hughen et al.*, 2007]).

2.3. U-Series Measurements

All analyses of U, Th, and Pa were made by isotope dilution. Most of the U-series measurements were made at the Lamont-Doherty Earth Observatory using a Thermo-Elemental Axiom, single collector, inductively coupled plasma–mass spectrometer (ICP-MS), with five additional analyses at the Woods Hole Oceanographic Institute using a Finnigan MAT Element I, single collector, and ICP-MS. All data are displayed, and differences between the methods and results from each laboratory are discussed in Table S2 in the supporting information.

The excess activities of ^{230}Th and ^{231}Pa, and their associated uncertainties, were calculated for each sample using the MATLAB script XSage, which is discussed fully by *Bourne et al.* [2012]. Contributions to these activities from supported and authigenic phases were calculated and removed by assuming an authigenic $^{234}U/^{238}U > 1$ and estimating a baseline detrital $^{238}U/^{232}Th$ ratio from samples without authigenic uranium [*Bourne et al.*, 2012]. We found that $^{238}U/^{232}Th = 0.6 \pm 0.1$ most represented the detrital composition of our cores; this is within the range suggested for the Atlantic [*Henderson and Anderson*, 2003; *McManus et al.*, 1998, 2004]. We also note that a sensitivity test of calculations using $^{238}U/^{232}Th = 0.5$, 0.6, and 0.7 resulted in $^{231}Pa/^{230}Th$ values within instrument error of each other for all depths in the three cores, and we therefore conclude that within this range, the choice of detrital value is not important for the data and time interval of this study. The XSage script also corrected the excess activities for radioactive decay, using the independently determined age models described in section 2.2, along with a Monte Carlo method to determine the age uncertainty contribution to the $^{231}Pa/^{230}Th$ uncertainties.

2.4. Flux Calculations

The flux of bulk sediment at each core site was calculated assuming that the vertical scavenging of ^{230}Th at a given core depth was equal to the production of ^{230}Th in the water column above [*Bacon*, 1984; *Francois et al.*, 2004].

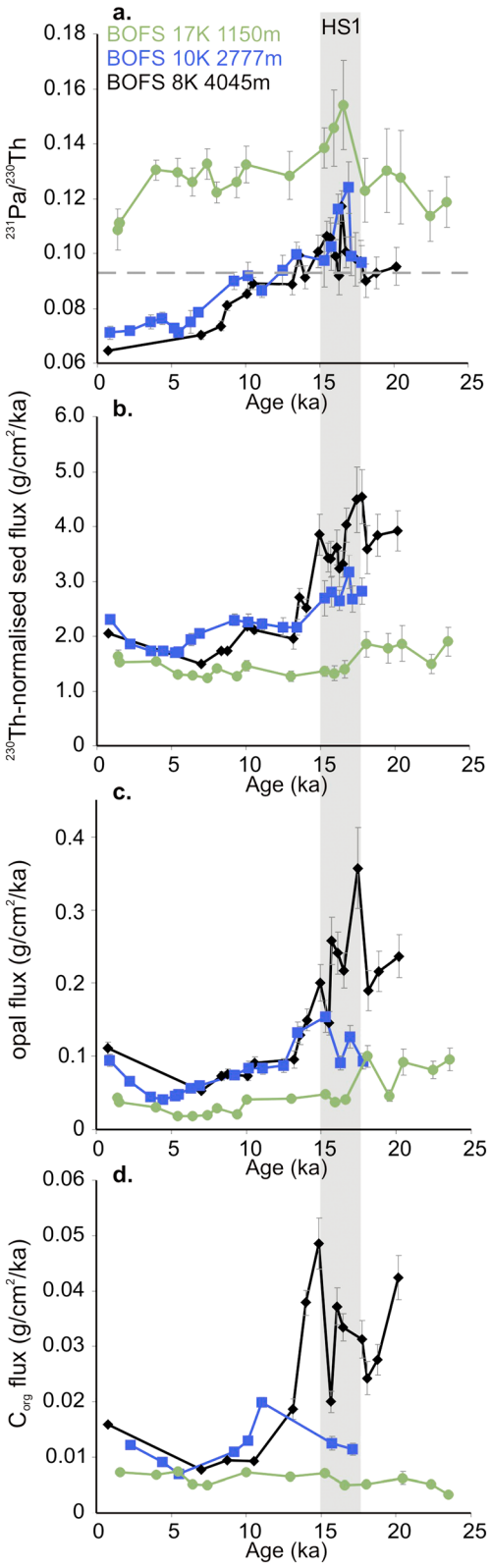

Based on the bulk sediment fluxes, the preserved opal fluxes were calculated from the fractional composition of the sediment, where % opal measurements were made on homogenized splits of each sample at Lamont-Doherty Earth Observatory, by alkaline extraction and molybdate-blue spectrophotometry [*Mortlock and Froelich*, 1989]. The preserved organic carbon fluxes were calculated using previously determined % C_{org} measurements published by *Manighetti and McCave* [1995].

3. Results

All new data generated in this study, on cores BOFS 17 K, 10 K, and 8 K, are plotted together in Figures 2a–2c and compared with the records of organic carbon flux (Figure 2d) [*Manighetti and McCave*, 1995]. The shallowest core, at intermediate water depth, BOFS 17 K (1150 m), recorded the highest ^{231}Pa/^{230}Th, consistently above the production ratio, and the lowest ^{230}Th-normalized bulk sediment fluxes, preserved opal fluxes and preserved organic carbon fluxes, throughout the last 24 ka. The two deep cores, BOFS 10 K (2777 m) and 8 K (4045 m), exhibit similar ^{231}Pa/^{230}Th records, with the lowest ratios during the Holocene and the highest between ~17.5 and 15 ka (grey bar). Prior to ~10 ka, all three cores recorded ^{231}Pa/^{230}Th within error of or above the production ratio, with peak ratios coinciding at ~17 ka. While the ^{230}Th-normalized bulk sediment fluxes, the preserved opal fluxes and the preserved organic carbon fluxes, were generally higher during the glacial and deglacial compared with the Holocene; the trends and timing of peak fluxes vary among the cores. Within the Holocene section of the three cores, the estimated sedimentary fluxes are generally similar, while the ^{231}Pa/^{230}Th of the two deep cores is significantly lower than in the shallow core.

Figure 2. Records of (a) ^{231}Pa/^{230}Th, (b) ^{230}Th-normalized bulk sediment fluxes, (c) opal fluxes, and (d) organic carbon fluxes [after *Manighetti et al.*, 1995] are displayed for each of the BOFS cores; 17 K (green), 10 K (blue), and 8 K (black). In Figure 2a, the horizontal dashed grey line represents the production ratio (0.093). The errors plotted are 2σ propagated internal errors calculated using the XSage MATLAB script [*Bourne et al.*, 2012], where the mean internal precision for ^{230}Th/^{229}Th and ^{233}Pa/^{231}Pa ratio measurements was <5% and <3% (2σ), respectively, and we included an error of ±8% on % opal analyses [*Mortlock and Froelich*, 1989]. The grey bar highlights Heinrich Stadial 1 (HS1). All data are presented in Tables S1 and S2 in the supporting information.

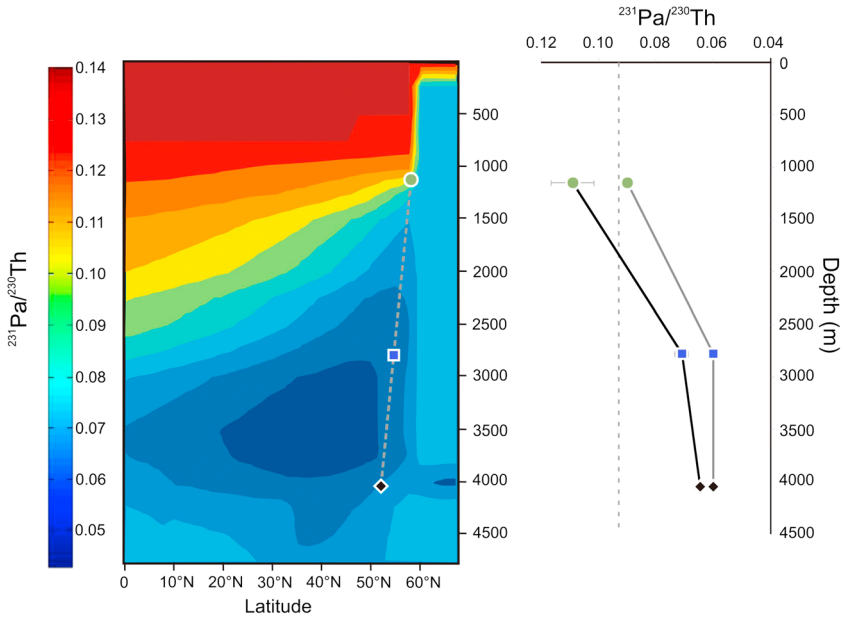

Figure 3. (left) A vertical transect exhibits model data output for the predicted sedimentary $^{231}Pa/^{230}Th$ in the North Atlantic [*Luo et al.*, 2010]. The depths and locations of each of the BOFS cores are displayed on the model output (17 K: green, 10 K: blue, and 8 K: black), and (right) the model data for each location (grey line) are compared with core-top values recorded at the BOFS cores (black line). The vertical dashed grey line represents the production ratio (0.093).

4. Discussion

Sediment core records of $^{231}Pa/^{230}Th$ spanning the last 20 ka from open ocean sites in the Atlantic have been interpreted in terms of changes in advection rate [*Gherardi et al.*, 2005, 2009; *Hall et al.*, 2006; *Lippold et al.*, 2012a; *McManus et al.*, 2004; *Negre et al.*, 2010; *Yu et al.*, 1996]. However, other factors such as particle type [e.g., *Chase et al.*, 2002], particle flux, and productivity [e.g., *Kumar et al.*, 1993; *Scholten et al.*, 2008] are also known to influence $^{231}Pa/^{230}Th$, complicating paleoceanographic interpretations of records closer to continental margins [*Lippold et al.*, 2012b]. More recently, rather than strictly limited to narrow zones proximal to continents, particle-scavenging gradients have been seen to apply to biogeographic zones associated with subtropical and subpolar regimes [*Broecker,* 2008; *Hayes et al.*, 2013]. In this section we discuss our data in the context of previously published $^{231}Pa/^{230}Th$ and $\overline{SS}$ data, and the potential controls on each, in order to evaluate the importance of scavenging and advection to and away from the BOFS transect.

4.1. Core-Top and Model Comparisons

Given the scarcity of ^{231}Pa and ^{230}Th water column profiles in the northern NE Atlantic, we compare core-top data from the BOFS cores with sedimentary $^{231}Pa/^{230}Th$ predicted using a 2-D scavenging model for the Atlantic (Figure 3) [*Luo et al.*, 2010]. There is observed spatial heterogeneity in productivity in this region [e.g., *Behrenfeld and Falkowski*, 1997]. This heterogeneity was not taken into account in the model and may be the cause of an offset in values between the model and the data; however, there is good agreement between the predicted and observed trends with depth in the water column, both exhibiting a decrease in $^{231}Pa/^{230}Th$ with increasing depth. This trend is recorded by core tops throughout the Atlantic [*Gherardi et al.*, 2009; *Lippold et al.*, 2011] and is generally consistent with advection control on $^{231}Pa/^{230}Th$ in the modern Atlantic Ocean, wherein dense deep waters are observed to flow faster [*Dickson et al.*, 1990], generating lower $^{231}Pa/^{230}Th$ than the intermediate depth water masses in the Atlantic. However, similar depth-dependent trends have also been found along the African margin [*Lippold et al.*, 2012b; *Scholten et al.*, 2008] and in the Arctic Ocean [*Hoffmann et al.*, 2013], where the oceanographic settings contrast with that of the NE Atlantic. These trends have been interpreted as reflecting stronger boundary scavenging closer to the African margin, and a depth-dependent relationship in dissolved concentrations relative to steady state, caused by reversible scavenging. Sediment $^{231}Pa/^{230}Th$ ratios above the production ratio, generated for shallow depths in the model, are interpreted as the result of dissolved ^{231}Pa concentrations above the predicted steady state

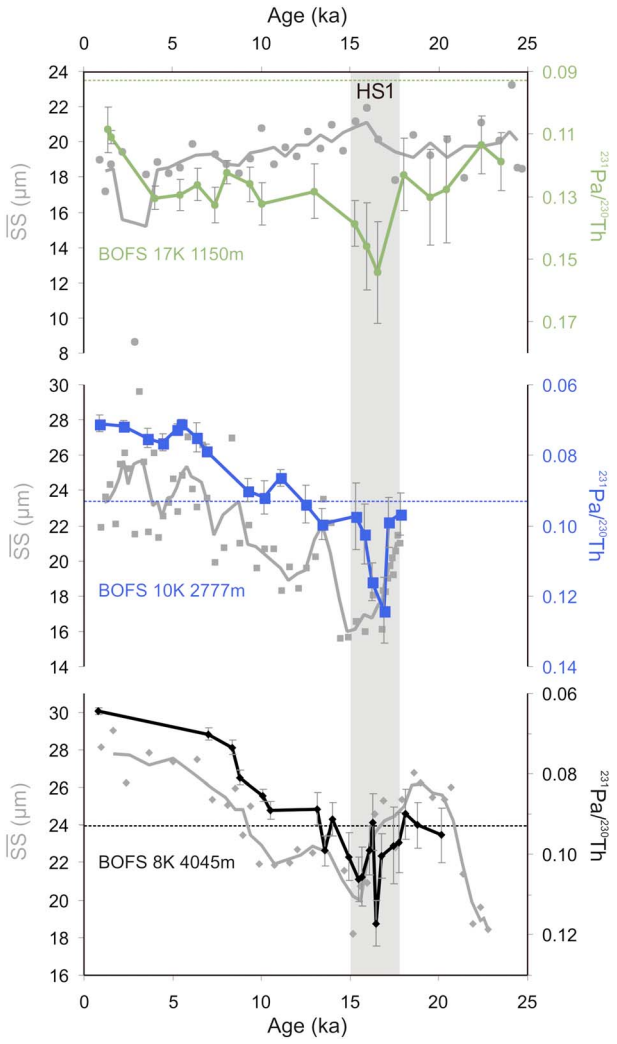

Figure 4. Records of $^{231}Pa/^{230}Th$ (17 K: green, 10 K: blue, and 8 K: black) are compared with $\overline{SS}$ data from *McCave et al.* [1995a] measured on the same cores (grey closed symbols), where the $\overline{SS}$ data have been smoothed using a three-point running mean (grey line). The errors for the $^{231}Pa/^{230}Th$ are plotted as 2σ propagated internal errors, and the errors for $\overline{SS}$ were calculated as <±2% based on % sortable silt, after *Bianchi et al.* [1999]; in this case, the error bars were smaller than the symbols. The grey bar is used to highlight Heinrich Stadial 1. The dashed lines on each graph indicate the production ratio (0.093).

concentration [*Luo et al.,* 2010], most likely brought about by mixing and limited lateral removal by advection. Lower silt grain sizes recorded at BOFS 17 K (Figure 4), relative to BOFS 10 K and 8 K, suggest slower advection rates at intermediate depths compared with the deep, resulting in $^{231}Pa/^{230}Th$ ratios that are more sensitive to local influences of particle scavenging. However, there must also be input of dissolved ^{231}Pa to this depth, by mixing, in order to generate core-top ratios above the production ratio. This effect is also recorded at other intermediate depth sites in the North Atlantic [*Gherardi et al.*, 2009]. Since all three sites sit below a region of high productivity today [*Behrenfeld and Falkowski*, 1997], we interpret the core-top $^{231}Pa/^{230}Th$ ratio at BOFS 17 K to be controlled by a combination of slow advection, mixing and high scavenging, and the ratios at BOFS 10 K and 8 K to be dominantly controlled by relatively fast advection.

4.2. Downcore $^{231}Pa/^{230}Th$ and $\overline{SS}$ Records

A comparison between $^{231}Pa/^{230}Th$ measured in this study and $\overline{SS}$ records measured on the same cores [*McCave et al.*, 1995a] highlights a number of similarities between the two proxies in the deep cores and differences in the intermediate water depth core (Figure 4). First, the increase in $^{231}Pa/^{230}Th$ recorded between ~17.5 and 16.5 ka in BOFS 10 K and 8 K was accompanied by a decrease in $\overline{SS}$. While both cores exhibit peak $^{231}Pa/^{231}Th$ ratios prior to $\overline{SS}$ minima, the sedimentary $^{231}Pa/^{230}Th$ remained high, either at or above the production ratio, while $\overline{SS}$ values remain low, until ~15 ka. Both proxies then recorded similar trends through the remaining deglacial and Holocene in BOFS 10 K and 8 K, with the Bølling–Allerød/Younger Dryas oscillation superimposed upon the $\overline{SS}$ trend [*McCave et al.*, 1995a]. A different relationship was recorded by BOFS 17 K; while the $^{231}Pa/^{230}Th$ peaked at a similar time to the deeper cores, this coincided with an increase in $\overline{SS}$ to peak values at ~16 ka, followed by a decline in values into the Holocene compared with relatively unchanging $^{231}Pa/^{230}Th$ values.

Both proxies have a kinematic control; however, they record different aspects of advection; $\overline{SS}$ records bottom current speed, while $^{231}Pa/^{230}Th$ integrates the water column, recording mean water mass advection rates. The decrease in $\overline{SS}$ in the two deep cores starting at ~17.5 ka has been interpreted as a result of reduced deep current advection speeds caused by freshwater discharge into the North Atlantic during Heinrich event 1 (H1) [*McCave et al.*, 1995a]. Similar shifts in $\overline{SS}$ at other locations support this inference [*Evans and Hall*, 2008;

Praetorius et al., 2008]. Here we refer to this period as Heinrich Stadial 1 (HS1, grey bar) as we do not have IRD provenance data to pinpoint the Heinrich event. An increase in $^{231}Pa/^{230}Th$ at the start of HS1 has also been interpreted in other cores across the North Atlantic as the result of a slowdown in advection rates [*Gherardi et al.*, 2005, 2009; *McManus et al.*, 2004]. The coincident shift in both proxies at the beginning of HS1 recorded by BOFS 8 K and 10 K, along with the peak $^{231}Pa/^{230}Th$ recorded by BOFS 17 K, is most simply interpreted as the result of slower deep current speeds and slower integrated water column advection rates at this time. However, since all three cores record $^{231}Pa/^{230}Th$ above the production ratio during HS1, we cannot solely relate these ratios to a slowdown in the advection rate. In the following section we discuss the possible causes of such high $^{231}Pa/^{230}Th$ ratios and their temporal relationship with advection changes inferred from $\overline{SS}$.

4.3. Hypotheses for $^{231}Pa/^{230}Th > 0.093$ During HS1

Here we discuss three additional potential controls on $^{231}Pa/^{230}Th$, which may have acted in conjunction with advection slowdown and could have been enhanced by environmental conditions during HS1: (i) particle flux or (ii) scavenging by opal and (iii) lateral input of dissolved ^{231}Pa.

4.3.1. High Bulk Sediment Fluxes and Nepheloid Layers

The ^{230}Th-normalized bulk sediment flux assumes that ^{230}Th produced in the water column is efficiently scavenged to the seafloor below the site of production [for further discussion, see *Francois et al.*, 2004; *McGee et al.*, 2010]. If particle fluxes are high enough, they may also efficiently scavenge ^{231}Pa [*Anderson et al.*, 1983b; *Kumar et al.*, 1993; *Lippold et al.*, 2012b; *Siddall et al.*, 2005]. The two deep BOFS cores record peak bulk sediment fluxes during HS1, with low fluxes to BOFS 17 K (Figure 2b). This difference is most likely related to the core site positions relative to the IRD belt [*Ruddiman*, 1977]. Due to the cyclonic nature of IRD deposition in the glacial North Atlantic, core sites on the southern part of the transect received more detrital material than those to the north, recorded as differences in magnetic susceptibility [*Manighetti et al.*, 1995; *Robinson et al.,* 1995]. However, the highest bulk sediment fluxes recorded at BOFS 8 K only approach 5 g cm^{-2} ka^{-1}, which are no greater than fluxes recorded by cores exhibiting an advection control on $^{231}Pa/^{230}Th$ [*Gherardi et al.*, 2009; *McManus et al.*, 2004]. If such sediment fluxes were capable of stripping excess ^{231}Pa from the water column, the resulting sediment $^{231}Pa/^{230}Th$ ratios could not have been sustained above the production ratio for the duration of HS1 by uranium decay alone. We infer that sediment fluxes during HS1 may have contributed to high $^{231}Pa/^{230}Th$ but are unlikely to be the primary cause of $^{231}Pa/^{230}Th > 0.093$.

Nepheloid layers result from the resuspension of fine sediment particles by bottom currents [*Jerlov*, 1953]. They have the potential to scavenge particle reactive elements from the water column [*Bacon and Rutgers van der Loeff*, 1989], with new evidence for enhanced ^{231}Pa and ^{230}Th scavenging emerging from the Atlantic GEOTRACES transects [*Deng et al.*, 2014]. Maps of present-day nepheloid layers indicate that fast flowing currents are associated with denser, thicker nepheloid layers [*Biscaye and Eittreim*, 1977; *McCave*, 1986]. Based on decreasing trends in $\overline{SS}$ recorded by BOFS 10 K and 8 K during HS1 (Figure 4), we infer that slowing of bottom currents likely resulted in reduced nepheloid layer production in this region and could therefore not have contributed to $^{231}Pa/^{230}Th > 0.093$ recorded by these cores.

4.3.2. Opal Scavenging

Chase et al. [2002] observed a similar efficiency of scavenging by biogenic opal for both ^{231}Pa and ^{230}Th, as opposed to a preference for ^{230}Th displayed by other particle types, resulting in $^{231}Pa/^{230}Th$ above the production ratio in opal-rich sediments found in the Southern Ocean. This relationship between opal and $^{231}Pa/^{230}Th$ has since been used to interpret paleoscavenging below opal productivity belts in the Southern Ocean [*Kumar et al.*, 1993] as well as the equatorial Atlantic and Pacific [*Bradtmiller et al.*, 2006, 2007; *Pichat et al.*, 2004]. Today, the Rockall Plateau lies beneath the North Atlantic high-productivity belt [*Behrenfeld and Falkowski*, 1997], where blooms include opal-producing organisms [*Honjo and Manganini*, 1993; *Jickells et al.*, 1996].

In this study we compare the preserved ^{230}Th-normalized opal fluxes (Figure 2c) with the sediment $^{231}Pa/^{230}Th$ ratios from the same samples (Figure 2a). We find that BOFS 17 K, while recording the highest $^{231}Pa/^{230}Th$, also recorded the lowest preserved opal concentrations and fluxes throughout the last 24 ka (Figure S1 in the supporting information). The only core to record opal fluxes significantly higher than core-top values, at the same time as peak $^{231}Pa/^{230}Th$ values, was BOFS 8 K. Preserved opal fluxes are not a

measure of opal rain but of burial after significant dissolution at the sediment-water interface [*McManus et al.*, 1995; *Van Cappellen et al.*, 2002]. High preserved opal fluxes coincide with high bulk sediment fluxes (Figure 2b). Given that opal makes up less than 8% of the sediment (Table S2 in the supporting information), high detrital input during HS1 most likely aided preservation of biogenic material due to more rapid burial and addition of dissolved aluminum to the pore waters [*Van Cappellen et al.*, 2002]. This preservation mechanism is supported by higher preserved organic carbon fluxes in BOFS 8 K glacial samples compared with BOFS 17 K (Figure 2d). Oxidative removal of sinking organic matter increases with depth in the water column [*Jahnke*, 1996] and should produce a decreasing trend with depth at the BOFS sites, opposite to that observed, if the organic concentration of the sediment was controlled by productivity and vertical flux rather than preservation.

We find mixed evidence from other studies with regard to opal productivity changes during HS1. It has generally been viewed as a time of low productivity [*Broecker et al.*, 1992; *Hemming*, 2004; *Ruddiman and McIntyre*, 1981], and throughout the North Atlantic, other sediment cores recorded either low preserved opal fluxes or progressively increasing fluxes through HS1 [*Gherardi et al.*, 2009; *Nave et al.*, 2007]. Yet others have discussed the potential for increased productivity [*Keigwin and Boyle*, 2008; *Sancetta*, 1992]. *Rashid and Boyle* [2007] reported deepening of the mixed layer in the central North Atlantic during HS1 which could have led to increased opal productivity, although this is unlikely to have affected the Rockall Plateau, since nearby NE Atlantic cores recorded strong surface stratification due to freshening [*Thornalley et al.*, 2011].

The core-top data for these sites indicates that modern productivity is sufficient to produce $^{231}Pa/^{230}Th > 0.093$ in BOFS 17 K, but advection is strong enough to dominate the signal in the two deeper cores (Figure 3). It is therefore possible that slower advection rates during HS1 could have resulted in elevated $^{231}Pa/^{230}Th$ throughout the water column without any increase in opal flux relative to the modern. It is important to note that if opal fluxes were elevated during HS1, this could have resulted in a transient peak in ratios above the production ratio but not in sustained $^{231}Pa/^{230}Th > 0.093$. A scenario, in which $^{231}Pa/^{230}Th$ ratios above the production ratio would be recorded in the North Atlantic during HS1, was predicted by an ocean circulation modeling study [*Siddall et al.*, 2007]. In the model, regions of high-particle flux were particularly sensitive to a circulation slowdown, since any remaining ^{231}Pa in the water column would be transported laterally by eddy diffusion to regions of high scavenging. Modern observations in the Pacific Ocean are also consistent with this result, where higher $^{231}Pa/^{230}Th$ has been observed in areas of enhanced scavenging of ^{231}Pa, initially along the basin margins [*Anderson et al.*, 1983b; *Lao et al.*, 1992], and more recently within the subpolar gyre [*Hayes et al.*, 2013].

4.3.3. Lateral Input of Dissolved ^{231}Pa

Considering mass balance requirements, irrespective of the scavenging intensity, the availability of transported ^{231}Pa must have increased during HS1 to allow the continued burial, at all three sites, of more ^{231}Pa than was produced locally. Based on the BOFS 17 K record, this must have been the case throughout the last 24 ka at intermediate depths on the Rockall Plateau. Using estimates of dissolved ^{231}Pa residence time in the open ocean on the order of $\tau = 50$ to 130 years [*Anderson et al.*, 1983a], and a horizontal eddy diffusion coefficient $K_H = 2 \times 10^3\ m^2\ s^{-1}$ [*Ledwell et al.*, 1998; *Sarmiento et al.*, 1982], the length scale over which ^{231}Pa can be transported by eddy diffusion, Δx, can be calculated using the equation $\Delta x = \sqrt{2K_H\tau}$ [*Roy-Barman*, 2009]. It is possible that dissolved ^{231}Pa could be laterally transported from ~2500 to 4000 km to the Rockall Plateau, i.e., the majority of the North Atlantic and Nordic Seas. This process is termed boundary scavenging [*Bacon et al.*, 1976; *Spencer et al.*, 1981], and today it is considered not to be an important sink for ^{231}Pa in the deep Atlantic due to fast advection rates [*Yu et al.*, 1996]; however, during a slowdown in advection rates, boundary scavenging may have become a significant process [*Siddall et al.*, 2007] and likely one that was not limited to marginal settings [*Hayes et al.*, 2013].

We suggest that, even without significantly increased opal scavenging relative to the modern, a slowdown in advection during HS1 could nevertheless have allowed transport via eddy diffusion of dissolved ^{231}Pa to the Rockall Plateau, where it was subsequently scavenged by high-particle fluxes. The comparison between the BOFS $^{231}Pa/^{230}Th$ records and other North Atlantic cores indicates that lateral input could have come from any direction during early HS1, when we observe peak $^{231}Pa/^{230}Th$, as cores from the North, South, and West recorded $^{231}Pa/^{230}Th$ below the production ratio at this time (Figure 5) and were therefore potential source regions for dissolved ^{231}Pa. This hypothesis is supported by model estimates, whereby similar particle

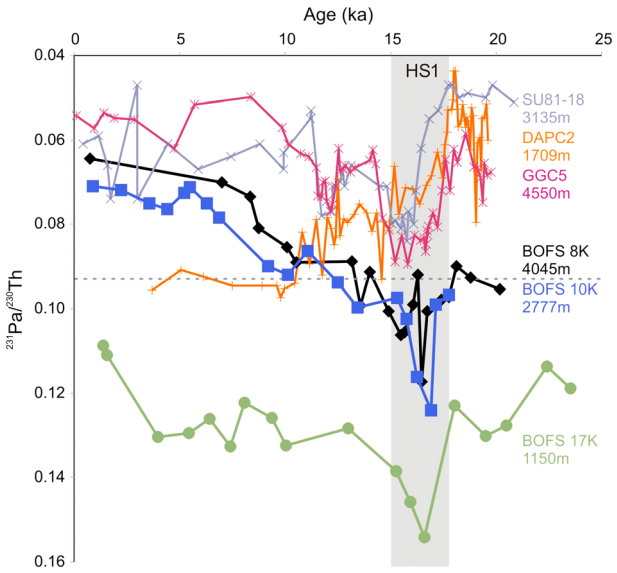

Figure 5. The $^{231}Pa/^{230}Th$ records for BOFS 17 K (green), 10 K (blue), and 8 K (black) are compared with other North Atlantic records from cores DAPC2 (orange; *Hall et al.*, 2006), SU81-18 (light blue; *Gherardi et al.*, 2005), and OCE326-GGC5 (purple; *McManus et al.*, 2004) across the deglacial period. The horizontal dashed grey line represents the production ratio (0.093), and the grey bar highlights Heinrich Stadial 1.

fluxes relative to modern values would have resulted in $^{231}Pa/^{230}Th$ above the production ratio at the Rockall Plateau [*Siddall et al.*, 2007].

An alternative lateral input source of dissolved ^{231}Pa to the Rockall Plateau may have been from the Nordic Seas. Today, ^{231}Pa and ^{230}Th activity measurements of Arctic seawater and sediment indicate that below permanent sea ice, scavenging of particle reactive elements is reduced [*Hoffmann and McManus*, 2007; *Moran et al.*, 2005]. *Moran et al.* [2005] calculated that 39% of the ^{231}Pa produced in the Arctic is advected through the Fram Strait into the Nordic Seas, compared with only 10% of ^{230}Th produced. Similar estimates have been made using Holocene and glacial Arctic sediment $^{231}Pa/^{230}Th$ [*Hoffmann and McManus*, 2007; *Hoffmann et al.*, 2013]. We suggest that during HS1, the increased sea ice cover over the Nordic Seas [*de Vernal and Hillaire-Marcel*, 2000] prevented scavenging of ^{231}Pa, which may have been subsequently advected to the NE Atlantic, either by eddy diffusion or by brine injection [*Meland et al.*, 2008], where it was then scavenged.

We currently have no way to distinguish between lateral input sources, or scavenging by opal relative to bulk sediment to account for the elevated ratios at all three sites, but it is clear that during HS1, the Rockall Plateau acted as a scavenging boundary for dissolved ^{231}Pa.

5. Summary and Implications

Prior to this study, it remained to be tested whether $^{231}Pa/^{230}Th$ records from sites below productive surface waters in the North Atlantic would be more sensitive to advection slowdown, as suggested by *Siddall et al.* [2007]. We have shown that three cores, taken from the northern NE Atlantic productivity belt, record $^{231}Pa/^{230}Th$ which, for the deep sites is dominantly controlled by advection today, but during HS1 exceeded the production ratio at all depths in the water column. The bulk sediment and preserved biogenic component fluxes do not allow us to quantify changes in scavenging to these cores across HS1, as we cannot determine the degree to which remineralization altered these fluxes. However, using $\overline{SS}$ as a proxy for bottom water current speed, we infer that during advection slowdown of deep waters, lateral input of dissolved ^{231}Pa was scavenged at the Rockall Plateau, without the need for increased particle fluxes relative to the present day. Despite the fact that our records sample a depth transect, with each core bathed by a different water mass during the glacial [*Yu et al.*, 2008], the trends in the two deep $^{231}Pa/^{230}Th$ records are similar over the last 20 ka, with all three sites recording a peak during HS1, indicating similar mechanisms acted.

This study does not inform on the degree to which advection slowed during HS1, but it does provide further support for the connection between deep circulation and climate change at this time, along with information on temporal changes in boundary scavenging in the productive northern NE Atlantic. We find that, while intermediate sites have been a constant sink for dissolved ^{231}Pa during the last 24 ka, deep sites allow removal of ^{231}Pa when advection rates are fast and act as a temporary sink when advection is slow. The data from this study are useful for understanding glacial budgets of ^{231}Pa export from the Atlantic and to inform sampling for nonscavenging-controlled $^{231}Pa/^{230}Th$ records.

Acknowledgments
We would like to thank Bob Anderson for the use of his lab and spike, Martin Fleisher, Pat Malone, Joanne Goudreau, Abel Guihou, and Laura Robinson for the guidance in U-series sample processing and analysis, and also Luke Skinner for the ^{14}C sample preparation and age model discussion. This work was funded in part by the Comer Science and Education Foundation and NSF grants OCE 0902985 and AGS 0936496 at Lamont-Doherty Earth Observatory and by NERC studentship NE/F007132/1 at the University of Cambridge.

References

Anderson, R. F., M. P. Bacon, and P. G. Brewer (1983a), Removal of ^{230}Th and ^{231}Pa from the open ocean, *Earth Planet. Sci. Lett.*, *62*(1), 7–23.
Anderson, R. F., M. P. Bacon, and P. G. Brewer (1983b), Removal of ^{230}Th and ^{231}Pa at ocean margins, *Earth Planet. Sci. Lett.*, *66*, 73–90.
Bacon, M. P. (1984), Glacial to interglacial changes in carbonate and clay sedimentation in the Atlantic Ocean estimated from ^{230}Th measurements, *Chem. Geol.*, *46*(2), 97–111.
Bacon, M. P., and R. F. Anderson (1982), Distribution of thorium isotopes between dissolved and particulate forms in the deep sea, *J. Geophys. Res.*, *87*(C3), 2045–2056, doi:10.1029/JC087iC03p02045.
Bacon, M. P., and M. M. Rutgers van der Loeff (1989), Removal of thorium-234 by scavenging in the bottom nepheloid layer of the ocean, *Earth Planet. Sci. Lett.*, *92*(2), 157–164.
Bacon, M., D. Spencer, and P. Brewer (1976), $^{210}Pb/^{226}Ra$ and $^{210}Po/^{210}Pb$ disequilibria in seawater and suspended particulate matter, *Earth Planet. Sci. Lett.*, *32*, 277–296.
Bard, E. (1988), Correction of accelerator mass spectrometry ^{14}C ages measured in planktonic foraminifera: Paleoceanographic implications, *Paleoceanography*, *3*(6), 635–695, doi:10.1029/PA003i006p00635.
Barker, S., T. Kiefer, and H. Elderfield (2004), Temporal changes in North Atlantic circulation constrained by planktonic foraminiferal shell weights, *Paleoceanography*, *19*, PA3008, doi:10.1029/2004PA001004.
Behrenfeld, M. J., and P. G. Falkowski (1997), Photosynthetic rates derived from satellite-based chlorophyll concentration, *Limnol. Oceanogr.*, *42*(1), 1–20.
Benway, H. M., J. F. McManus, D. W. Oppo, and J. L. Cullen (2010), Hydrographic changes in the eastern subpolar North Atlantic during the last deglaciation, *Quat. Sci. Rev.*, *29*(23–24), 3336–3345.
Bertram, C. J., H. Elderfield, N. J. Shackleton, and J. A. MacDonald (1995), Cadmium/calcium and carbon isotope reconstructions of the glacial northeast Atlantic Ocean, *Paleoceanography*, *10*(3), 563–578, doi:10.1029/94PA03058.
Bianchi, G., I. R. Hall, I. McCave, and L. Joseph (1999), Measurement of the sortable silt current speed proxy using the Sedigraph 5100 and Coulter Multisizer IIe: Precision and accuracy, *Sedimentology*, *46*(6), 1001–1014.
Biscaye, P. E., and S. L. Eittreim (1977), Suspended particulate loads and transports in the nepheloid layer of the abyssal Atlantic Ocean, *Mar. Geol.*, *23*(1–2), 155–172.
Bourne, M. D., A. L. Thomas, C. Mac Niocaill, and G. M. Henderson (2012), Improved determination of marine sedimentation rates using $^{230}Th_{xs}$, *Geochem. Geophys. Geosyst.*, *13*, Q09017, doi:10.1029/2012GC004295.
Bradtmiller, L., R. Anderson, M. Fleisher, and L. Burckle (2006), Diatom productivity in the equatorial Pacific Ocean from the last glacial period to the present: A test of the silicic acid leakage hypothesis, *Paleoceanography*, *21*, PA4201, doi:10.1029/2006PA001282.
Bradtmiller, L., R. Anderson, M. Fleisher, and L. Burckle (2007), Opal burial in the equatorial Atlantic Ocean over the last 30 ka: Implications for glacial-interglacial changes in the ocean silicon cycle, *Paleoceanography*, *22*, PA4216, doi:10.1029/2007PA001443.
Broecker, W. (2008), Excess sediment ^{230}Th: Transport along the sea floor or enhanced water column scavenging?, *Global Biogeochem. Cycles*, *22*, GB1006, doi:10.1029/2007GB003057.
Broecker, W., G. Bond, M. Klas, E. Clark, and J. McManus (1992), Origin of the northern Atlantic's Heinrich events, *Clim. Dyn.*, *6*(3–4), 265–273.
Brown, L., G. T. Cook, A. B. MacKenzie, and J. Thomson (2001), Radiocarbon age profiles and size dependency of mixing in northeast Atlantic sediments, *Radiocarbon*, *43*, 929–937.
Chase, Z., R. F. Anderson, M. Q. Fleisher, and P. W. Kubik (2002), The influence of particle composition and particle flux on scavenging of Th, Pa and Be in the ocean, *Earth Planet. Sci. Lett.*, *204*(1–2), 215–229.
Curry, W. B., and D. W. Oppo (2005) Glacial water mass geometry and the distribution of $\delta^{13}C$ of ΣCO2 in the western Atlantic Ocean, *Paleoceanography*, *20*, PA1017, doi:10.1029/2004PA001021.
Clark, P. U., N. G. Pisias, T. F. Stocker, and A. J. Weaver (2002), The role of the thermohaline circulation in abrupt climate change, *Nature*, *415*(6874), 863–869.
Deng, F., A. L. Thomas, M. J. Rijkenberg, and G. M. Henderson (2014), Controls on seawater ^{231}Pa, ^{230}Th and ^{232}Th concentrations along the flow paths of deep waters in the Southwest Atlantic, *Earth Planet. Sci. Lett.*, *390*, 93–102.
de Vernal, A., and C. Hillaire-Marcel (2000), Sea-ice cover, sea-surface salinity and halo-/thermocline structure of the northwest North Atlantic: Modern versus full glacial conditions, *Quat. Sci. Rev.*, *19*(1–5), 65–85.
Dickson, R., E. Gmitrowicz, and A. Watson (1990), Deep-water renewal in the northern North Atlantic, *Nature*, *344*, 848–850.
Dokken, T. M., and E. Jansen (1999), Rapid changes in the mechanism of ocean convection during the last glacial period, *Nature*, *401*(6752), 458–461.
Duplessy, J. C., N. J. Shackleton, R. G. Fairbanks, L. Labeyrie, D. Oppo, and N. Kallel (1988), Deepwater source variations during the last climatic cycle and their impact on the global deepwater circulation, *Paleoceanography*, *3*(3), 343–360, doi:10.1029/PA003i003p00343.
Evans, H. K., and I. R. Hall (2008), Deepwater circulation on Blake Outer Ridge (western North Atlantic) during the Holocene, Younger Dryas, and Last Glacial Maximum, *Geochem. Geophys. Geosyst.*, *9*, Q03023, doi:10.1029/2007GC001771.
Francois, R., M. Frank, M. M. Rutgers van der Loeff, and M. P. Bacon (2004), ^{230}Th normalization: An essential tool for interpreting sedimentary fluxes during the late Quaternary, *Paleoceanography*, *19*, PA1018, doi:10.1029/2003PA000939.
Ganopolski, A., and S. Ramstorf (2001), Rapid changes of glacial climate model simulated in coupled climate model, *Nature*, *409*, 153–157.
Gherardi, J.-M., L. Labeyrie, J. F. McManus, R. Francois, L. C. Skinner, and E. Cortijo (2005), Evidence from the Northeastern Atlantic basin for variability in the rate of the meridional overturning circulation through the last deglaciation, *Earth Planet. Sci. Lett.*, *240*(3–4), 710–723.
Gherardi, J. M., L. Labeyrie, S. Nave, R. Francois, J. F. McManus, and E. Cortijo (2009), Glacial-interglacial circulation changes inferred from $^{231}Pa/^{230}Th$ sedimentary record in the North Atlantic region, *Paleoceanography*, *24*, PA2204, doi:10.1029/2008PA001696.
Hall, I. R., S. B. Moran, R. Zahn, P. C. Knutz, C.-C. Shen, and R. L. Edwards (2006), Accelerated drawdown of meridional overturning in the late-glacial Atlantic triggered by transient pre-H event freshwater perturbation, *Geophys. Res. Lett.*, *33*, L16616, doi:10.1029/2006GL026239.
Hayes, C. T., R. F. Anderson, S. L. Jaccard, R. François, M. Q. Fleisher, M. Soon, and R. Gersonde (2013), A new perspective on boundary scavenging in the North Pacific Ocean, *Earth Planet. Sci. Lett.*, *369–370*, 86–97.
Hemming, S. R. (2004), Heinrich events: Massive late Pleistocene detritus layers of the North Atlantic and their global climate imprint, *Rev. Geophys.*, *42*, RG1005, doi:10.1029/2003RG000128.
Hemming, S., W. Broecker, W. Sharp, G. Bond, R. Gwiazda, J. McManus, M. Klas, and I. Hajdas (1998), Provenance of Heinrich layers in core V28-82, northeastern Atlantic: $^{40}Ar/^{39}Ar$ ages of ice-rafted hornblende, Pb isotopes in feldspar grains, and Nd–Sr–Pb isotopes in the fine sediment fraction, *Earth Planet. Sci. Lett.*, *164*(1), 317–333.
Henderson, G. M., and R. F. Anderson (2003), The U-series toolbox for paleoceanography, *Rev. Mineral. Geochem.*, *52*(1), 493–531.
Hoffmann, S., and J. McManus (2007), Is there a ^{230}Th deficit in Arctic sediments?, *Earth Planet. Sci. Lett.*, *258*(3–4), 516–527.

Hoffmann, S. S., J. F. McManus, W. B. Curry, and L. S. Brown-Leger (2013), Persistent export of ^{231}Pa from the deep central Arctic Ocean over the past 35,000 years, *Nature*, *497*(7451), 603–606.
Honjo, S., and S. J. Manganini (1993), Annual biogenic particle fluxes to the interior of the North Atlantic Ocean; studied at 34 N 21 W and 48 N 21 W, *Deep Sea Res. Topic. Stud. Oceanogr.*, *40*(1), 587–607.
Hughen, K. A., M. G. L. Baillie, E. Bard, J. W. Beck, C. J. H. Bertrand, P. G. Blackwell, C. E. Buck, G. S. Burr, K. B. Cutler, and P. E. Damon (2007), Marine04 marine radiocarbon age calibration, 0-26 cal kyr BP, *Radiocarbon*, *46*(3), 1059–1086.
Jahnke, R. A. (1996), The global ocean flux of particulate organic carbon: Areal distribution and magnitude, *Global Biogeochem. Cycles*, *10*(1), 71–88, doi:10.1029/95GB03525.
Jerlov, N. G. (1953), Particle distribution in the ocean, *Reports of the Swedish Deep-Sea Expedition*, *3*, 73–97.
Jickells, T., P. Newton, P. King, R. Lampitt, and C. Boutle (1996), A comparison of sediment trap records of particle fluxes from 19 to 48 N in the northeast Atlantic and their relation to surface water productivity, *Deep Sea Res., Part I*, *43*(7), 971–986.
Keigwin, L. D., and E. A. Boyle (2008), Did North Atlantic overturning halt 17,000 years ago?, *Paleoceanography*, *23*, PA1101, doi:10.1029/2007PA001500.
Knutz, P. C., R. Zahn, and I. R. Hall (2007), Centennial-scale variability of the British Ice Sheet: Implications for climate forcing and Atlantic meridional overturning circulation during the last deglaciation, *Paleoceanography*, *22*, PA1207, doi:10.1029/2006PA001298.
Kretschmer, S., W. Geibert, M. M. Rutgers van der Loeff, and G. Mollenhauer (2010), Grain size effects on $^{230}Th_{xs}$ inventories in opal-rich and carbonate-rich marine sediments, *Earth Planet. Sci. Lett.*, *294*(1), 131–142.
Kretschmer, S., W. Geibert, M. M. Rutgers van der Loeff, C. Schnabel, S. Xu, and G. Mollenhauer (2011), Fractionation of ^{230}Th, ^{231}Pa, and ^{10}Be induced by particle size and composition within an opal-rich sediment of the Atlantic Southern Ocean, *Geochim. Cosmochim. Acta*, *75*(22), 6971–6987.
Kumar, N., R. Gwiazda, R. Anderson, and P. Froelich (1993), ^{231}Pa/^{230}Th ratios in sediments as a proxy for past changes in Southern Ocean productivity, *Nature*, *362*(6415), 45–48.
Kwon, E. Y., M. P. Hain, D. M. Sigman, E. D. Galbraith, J. L. Sarmiento, and J. Toggweiler (2012), North Atlantic ventilation of "southern-sourced" deep water in the glacial ocean, *Paleoceanography*, *27*, PA2208, doi:10.1029/2011PA002211.
Lao, Y., R. F. Anderson, and W. S. Broecker (1992), Boundary scavenging and deep-sea sediment dating: Constraints from excess ^{230}Th and ^{231}Pa, *Paleoceanography*, *7*(6), 783–798, doi:10.1029/92PA02042.
Ledbetter, M. T. (1986), A late Pleistocene time series of bottom-current speed in the Vema Channel, *Palaeogeogr. Palaeoclimatol. Palaeoecol.*, *53*(1), 97–105.
Ledwell, J. R., A. J. Watson, and C. S. Law (1998), Mixing of a tracer in the pycnocline, *J. Geophys. Res.*, *103*(C10), 21,499–21,529, doi:10.1029/98JC01738.
LeGrande, A., G. Schmidt, D. Shindell, C. Field, R. Miller, D. Koch, G. Faluvegi, and G. Hoffmann (2006), Consistent simulations of multiple proxy responses to an abrupt climate change event, *Proc. Natl. Acad. Sci. U. S. A.*, *103*(4), 837–842.
Lippold, J., J. M. Gherardi, and Y. Luo (2011), Testing the ^{231}Pa/^{230}Th paleocirculation proxy: A data versus 2D model comparison, *Geophys. Res. Lett.*, *38*, L20603, doi:10.1029/2011GL049282.
Lippold, J., S. Mulitza, G. Mollenhauer, S. Weyer, D. Heslop, and M. Christl (2012a), Boundary scavenging at the East Atlantic margin does not negate use of ^{231}Pa/^{230}Th to trace Atlantic overturning, *Earth Planet. Sci. Lett.*, *333–334*, 317–331.
Lippold, J., Y. Luo, R. Francois, S. E. Allen, J. Gherardi, S. Pichat, B. Hickey, and H. Schulz (2012b), Strength and geometry of the glacial Atlantic meridional overturning circulation, *Nat. Geosci.*, *5*, 813–816.
Liu, Z., et al. (2009), Transient simulation of last deglaciation with a new mechanism for Bølling-Allerød warming, *Science*, *325*(5938), 310–314.
Luo, Y., R. Francois, and S. Allen (2010), Sediment ^{231}Pa/^{230}Th as a recorder of the rate of the Atlantic meridional overturning circulation: Insights from a 2-D model, *Ocean Sci*, *6*, 381–400.
Lynch-Stieglitz, J., et al. (2007), Atlantic meridional overturning circulation during the Last Glacial Maximum, *Science*, *316*(5821), 66–69.
Manabe, S., and R. J. Stouffer (1997), Coupled ocean-atmosphere model response to freshwater input: Comparison to Younger Dryas Event, *Paleoceanography*, *12*(2), 321–336, doi:10.1029/96PA03932.
Manighetti, B., and I. McCave (1995), Depositional fluxes, palaeoproductivity, and ice rafting in the NE Atlantic over the past 30 ka, *Paleoceanography*, *10*(3), 579–592, doi:10.1029/94PA03057.
Manighetti, B., I. N. McCave, M. A. Maslin, and N. J. Shackleton (1995), Chronology for climate change: Developing age models for the Biogeochemical Ocean Flux Study cores, *Paleoceanography*, *10*(3), 513–525, doi:10.1029/94PA03062.
Marchal, O., R. François, T. F. Stocker, and F. Joos (2000), Ocean thermohaline circulation and sedimentary ^{231}Pa/^{230}Th ratio, *Paleoceanography*, *15*(6), 625–641, doi:10.1029/2000PA000496.
McCave, I. N. (1986), Local and global aspects of the bottom nepheloid layers in the world ocean, *Neth. J. Sea Res.*, *20*(2–3), 167–181.
McCave, I. N. (1989), Cruise report, RRS Discovery cruise 184, BOFS 1989 Leg 3, Dept. of Earth Sciences(Cambridge), 38 + figs and tables.
McCave, I. N., and I. R. Hall (2006), Size sorting in marine muds: Processes, pitfalls, and prospects for paleoflow-speed proxies, *Geochem. Geophys. Geosyst.*, *7*, Q10N05, doi:10.1029/2006GC001284.
McCave, I. N., B. Manighetti, and N. Beveridge (1995a), Circulation in the glacial North Atlantic inferred from grain-size measurements, *Nature*, *374*(6518), 149–152.
McCave, I. N., B. Manighetti, and S. G. Robinson (1995b), Sortable silt and fine sediment size/composition slicing: Parameters for palaeocurrent speed and palaeoceanography, *Paleoceanography*, *10*(3), 593–610, doi:10.1029/94PA03039.
McGee, D., F. Marcantonio, J. F. McManus, and G. Winckler (2010), The response of excess ^{230}Th and extraterrestrial ^{3}He to sediment redistribution at the Blake Ridge, western North Atlantic, *Earth Planet. Sci. Lett.*, *299*(1), 138–149.
McManus, J., D. E. Hammond, W. M. Berelson, T. E. Kilgore, D. J. Demaster, O. G. Ragueneau, and R. W. Collier (1995), Early diagenesis of biogenic opal: Dissolution rates, kinetics, and paleoceanographic implications, *Deep Sea Res. Topic. Stud. Oceanogr.*, *42*(2–3), 871–903.
McManus, J. F., R. F. Anderson, W. S. Broecker, M. Q. Fleisher, and S. M. Higgins (1998), Radiometrically determined sedimentary fluxes in the sub-polar North Atlantic during the last 140,000 years, *Earth Planet. Sci. Lett.*, *155*(1), 29–43.
McManus, J. F., R. Francois, J.-M. Gherardi, L. D. Keigwin, and S. Brown-Leger (2004), Collapse and rapid resumption of Atlantic meridional circulation linked to deglacial climate changes, *Nature*, *428*(6985), 834–837.
Mehta, A. J., and J. V. Letter Jr. (2013), Comments on the transition between cohesive and cohesionless sediment bed exchange, *Estuarine Coastal Shelf Sci.*, *131*, 319–324.
Meland, M. Y., T. M. Dokken, E. Jansen, and K. Hevrøy (2008), Water mass properties and exchange between the Nordic seas and the northern North Atlantic during the period 23–6 ka: Benthic oxygen isotopic evidence, *Paleoceanography*, *23*, PA1210, doi:10.1029/2007PA001416.
Moran, S., R. Kelly, K. Hagstrom, J. Smith, J. Grebmeier, L. Cooper, G. Cota, J. Walsh, N. Bates, and D. Hansell (2005), Seasonal changes in POC export flux in the Chukchi Sea and implications for water column-benthic coupling in Arctic shelves, *Deep Sea Res. Topic. Stud. Oceanogr.*, *52*(24–26), 3427–3451.

Mortlock, R. A., and P. N. Froelich (1989), A simple method for the rapid determination of biogenic opal in pelagic marine sediments, *Deep Sea Res. Oceanogr. Res. Paper.*, *36*(9), 1415–1426.
Nave, S., L. Labeyrie, J. Gherardi, N. Caillon, E. Cortijo, C. Kissel, and F. Abrantes (2007), Primary productivity response to Heinrich events in the North Atlantic Ocean and Norwegian Sea, *Paleoceanography*, *22*, PA3216, doi:10.1029/2006PA001335.
Negre, C., R. Zahn, A. L. Thomas, P. Masqué, G. M. Henderson, G. Martínez-Méndez, I. R. Hall, and J. L. Mas (2010), Reversed flow of Atlantic deep water during the Last Glacial Maximum, *Nature*, *468*(7320), 84–88.
Oppo, D. W., and S. J. Lehman (1993), Mid-depth circulation of the subpolar North Atlantic during the Last Glacial Maximum, *Science*, *259*(5098), 1148–1152.
Peltier, W. R., G. Vettoretti, and M. Stastna (2006), Atlantic meridional overturning and climate response to Arctic Ocean freshening, *Geophys. Res. Lett.*, *33*, L06713, doi:10.1029/2005GL025251.
Pichat, S., K. W. W. Sims, R. François, J. F. McManus, S. Brown Leger, and F. Albarède (2004), Lower export production during glacial periods in the equatorial Pacific derived from $(^{231}Pa/^{230}Th)_{xs,0}$ measurements in deep-sea sediments, *Paleoceanography*, *19*, PA4023, doi:10.1029/2003PA000994..
Praetorius, S. K., J. F. McManus, D. W. Oppo, and W. B. Curry (2008), Episodic reductions in bottom-water currents since the last ice age, *Nat. Geosci.*, *1*, 449–452.
Ramsey, C. B. (2001), Development of the radiocarbon calibration program, *Radiocarbon*, *43.2A*, 355–363.
Rashid, H., and E. A. Boyle (2007), Mixed-layer deepening during Heinrich events: A multi-planktonic foraminiferal $\delta^{18}O$ approach, *Science*, *318*(5849), 439–441.
Robinson, S. G., M. A. Maslin, and I. N. McCave (1995), Magnetic susceptibility variations in Upper Pleistocene deep-sea sediments of the NE Atlantic: Implications for ice rafting and paleocirculation at the last glacial maximum, *Paleoceanography*, *10*(2), 221–250, doi:10.1029/94PA02683.
Roy-Barman, M. (2009), Modelling the effect of boundary scavenging on Thorium and Protactinium profiles in the ocean, *Biogeosci. Discuss.*, *6*(4), 7853.
Ruddiman, W. F. (1977), Late Quaternary deposition of ice-rafted sand in the subpolar North Atlantic (lat 40 to 65 N), *Geol. Soc. Am. Bull.*, *88*(12), 1813–1827.
Ruddiman, W. F., and A. McIntyre (1981), The mode and mechanism of the last deglaciation: Oceanic evidence, *Quat. Res.*, *16*(2), 125–134.
Sancetta, C. (1992), Comparison of phytoplankton in sediment trap time series and surface sediments along a productivity gradient, *Paleoceanography*, *7*(2), 183–194, doi:10.1029/92PA00156.
Sarmiento, J., C. Rooth, and W. Broecker (1982), Radium 228 as a tracer of basin wide processes in the abyssal ocean, *J. Geophys. Res.*, *87*(C12), 9694–9698, doi:10.1029/JC087iC12p09694.
Sarnthein, M., et al. (1995), Variations in Atlantic surface ocean paleoceanography, 50°-80°N: A time-slice record of the last 30,000 years, *Paleoceanography*, *10*(6), 1063–1094, doi:10.1029/95PA01453.
Scholten, J. C., J. Fietzke, A. Mangini, C. D. Garbe-Schonberg, A. Eisenhauer, R. Schneider, and P. Stoffers (2008), Advection and scavenging: Effects on ^{230}Th and ^{231}Pa distribution off Southwest Africa, *Earth Planet. Sci. Lett.*, *271*(1–4), 159–169.
Siddall, M., G. M. Henderson, N. R. Edwards, M. Frank, S. A. Müller, T. F. Stocker, and F. Joos (2005), $^{231}Pa/^{230}Th$ fractionation by ocean transport, biogenic particle flux and particle type, *Earth Planet. Sci. Lett.*, *237*(1–2), 135–155.
Siddall, M., T. F. Stocker, G. M. Henderson, F. Joos, M. Frank, N. R. Edwards, S. P. Ritz, and S. A. Müller (2007), Modeling the relationship between $^{231}Pa/^{230}Th$ distribution in North Atlantic sediment and Atlantic meridional overturning circulation, *Paleoceanography*, *22*, PA2214, doi:10.1029/2006PA001358.
Spencer, D., M. Bacon, and P. Brewer (1981), Models of the distribution of ^{210}Pb in a section across the North Equatorial Atlantic Ocean, *J. Mar. Res.*, *39*(1), 119–138.
Stuut, J.-B. W., M. A. Prins, and J. H. F. Jansen (2002), Fast reconnaissance of carbonate dissolution based on the size distribution of calcareous ooze on Walvis Ridge, SE Atlantic Ocean, *Mar. Geol.*, *190*(3–4), 581–589.
Thornalley, D. J. R., H. Elderfield, and I. N. McCave (2011), Reconstructing North Atlantic deglacial surface hydrography and its link to the Atlantic overturning circulation, *Global Planet. Change*, *79*(3), 163–175.
Timmermann, A., U. Krebs, F. Justino, H. Goosse, and T. Ivanochko (2005), Mechanisms for millennial-scale global synchronization during the last glacial period, *Paleoceanography*, *20*, PA4008, doi:10.1029/2004PA001090.
Van Cappellen, P., S. Dixit, and J. van Beusekom (2002), Biogenic silica dissolution in the oceans: Reconciling experimental and field-based dissolution rates, *Global Biogeochem. Cycles*, *16*(4), 1075, doi:10.1029/2001GB001431.
Vellinga, M., and R. Wood (2002), Global climatic impacts of a collapse of the Atlantic thermohaline circulation, *Clim. Change*, *54*(3), 251–267.
Waelbroeck, C., J. C. Duplessy, E. Michel, L. Labeyrie, D. Paillard, and J. Duprat (2001), The timing of the last deglaciation in North Atlantic climate records, *Nature*, *412*(6848), 724–727.
Yu, E.-F., R. Francois, and M. P. Bacon (1996), Similar rates of modern and last-glacial ocean thermohaline circulation inferred from radiochemical data, *Nature*, *379*(6567), 689–694.
Yu, J., H. Elderfield, and A. M. Piotrowski (2008), Seawater carbonate ion-[delta]13C systematics and application to glacial-interglacial North Atlantic ocean circulation, *Earth Planet. Sci. Lett.*, *271*(1–4), 209–220.
Zhang, R., and T. L. Delworth (2005), Simulated tropical response to a substantial weakening of the atlantic thermohaline circulation, *J. Clim.*, *18*(12), 1853–1860.